Communications in Physics, Vol. 27, No. 4 (2017), pp. 317-326
DOI:10.15625/0868-3166/27/4/10899

ON-CHIP ZnO NANOFIBERS PREPARED BY ELECTROSPINNING METHOD FOR NO_2 GAS DETECTION

NGUYEN VAN HOANG[1,2], NGUYEN VAN DUNG[1], DO QUANG DAT[1], QUAN THI MINH NGUYET[1], CHU MANH HUNG[1,†] AND NGUYEN VAN HIEU[1,†]

[1]*International Training Institute for Materials Science (ITIMS), Hanoi University of Science and Technology (HUST), No. 1, Dai Co Viet Street, Hanoi, Vietnam*

[2]*Department of Materials Science and Engineering, Le Quy Don Technical University, No. 236 Hoang Quoc Viet Stress, Hanoi, Vietnam*

[†]*E-mail:* mhchu@itims.edu.vn; hieu@itims.edu.vn

Received 17 November 2017
Accepted for publication 20 December 2017
Published 31 December 2017

Abstract. *In the present study, on-chip ZnO nanofibers were fabricated by means of the electrospinning technique followed by a calcination process at 600˚C towards the gas sensor application. The morphology, composition, and crystalline structure of the as-spun and annealed ZnO nanofibers were investigated by field emission scanning electron microscopy (FESEM), energy dispersive X-ray (EDX), and X-ray diffraction (XRD), respectively. The findings show that spider-net like ZnO nanofibers with a diameter of 60 – 100 nm were successfully synthesized without any incorporation of impurities into the nanofibers. The FESEM images also reveal that each nanofiber is composed of many nanograins. The combination of experimental and calculated X-ray diffraction data indicate that ZnO nanofibers were crystallized in hexagonal wurtzite structure. For the gas sensing device application, the ZnO nanofibers-based sensors were tested with the nitrogen dioxide gas in the temperature range of 200˚C to 350˚C and concentrations from 2.5 ppm to 10 ppm. The sensing property results indicate that at the optimal working temperature of 300˚C the ZnO nanofibers-based sensors exhibited a maximum response of 30 and 166 times on exposure of 2.5 and 10 ppm NO_2 gas, respectively. The presence of nanograins within nanofibers, which results in further intensification of the resistance modulation, is responsible for such high gas response.*

Keywords: zinc oxide, nanofibers, electrospinning, NO_2 sensing.

Classification numbers: 81.07.Bc; 81.05.Hd.

I. INTRODUCTION

Nitrogen dioxide (NO_2) is usually generated by combustion processes and automobiles. This is known as one of the main toxic gaseous pollutants, which directly affect human health and environment at a very low concentration level. For instance, long-term exposure to NO_2 gas can damage the lung function; and the presence of NO_2 also causes the acid rain [1, 2]. Therefore, it is indispensable to develop high sensitive sensors for early detection and monitoring of NO_2 gas at a low concentration of ppm level. Many nanostructures like nanowires, nanorods, nanotubes and nanofibers can be used to enhance the sensing capability of chemical sensors [1, 3–5]. Among these nanostructures, nanofibers (NFs) are the most promising one because of their large surface to volume ratio and enormous grain boundary area. In the context of growth method, electrospinning is a simple, versatile and low-cost technique to fabricate continuous NFs of polymers, ceramics, semiconductors, and their composites [2]. Several semiconductor nanofiber types such as CuO, SnO_2, TiO_2, and ZnO [6] have been recently prepared by using such method. Among these semiconducting metal oxides, ZnO NFs, the n-type semiconductor with a wide direct band gap of 3.37 eV, are one of the most promising materials for gas sensors owing to their thermal-chemical stability under standard operating environment, high conductivity, and non-toxic properties.

Through the literature review, researchers have reported on electrospun ZnO NFs, which were obtained from the precursor solution mixing with either polyvinylpyrrolidone (PVP) or polyvinyl alcohol (PVA) and collected on silicon substrate and aluminum foil [4, 7]. Regarding the gas sensor application, the ZnO NFs also exhibited a good sensing performance. Namely, ZnO NFs as a gas sensing layer show a high response to H_2 [8] and NH_3 [9]. However, there have been only few reports on the investigation of the gas sensing property of the ZnO NF-based sensor to NO_2 gas [1, 5]. For example, Z. U. Abideen *et al.* [5] synthesized ZnO NFs on metal collectors with a stationary mode using electrospinning method, followed by calcination in the air for 5h at 500˚C. And then, ZnO NFs were sputtered with Ti and Pt to fabricate the sensor device for gas testing. The NO_2 gas response of such sensor is rather good, but it should work at high operating temperature of 400˚C

Herein, ZnO NFs were successfully developed directly on-chip via the electrospinning method on a rotary collector mode. NO_2 gas sensing capabilities of synthesized sensors were also tested in the temperature range of 200˚C to 350˚C and concentrations between 2.5 ppm and 10 ppm. The nanofibers consisting of small nanograins showed highly sensing properties to NO_2 gas at the optimal temperature of 300˚C

II. EXPERIMENT

On-chip fabrication of ZnO NFs by the electrospinning method is illustrated in Fig. 1. First, Zinc acetate $Zn(CH_3COO)_2$ $.2H_2O$ ($Zn(Ac)_2$) and PVA (purchased from Sigma-Aldrich and Merck corporations) were dissolved in the distilled water using a magnetic stirrer to form a homogeneous solution. By using a commercial electrospinning unit (TL – 01 Electrospinning, Tong Li Tech), the percursor solution was subsequently ejected from stainless needles (No. 7) of the syringe equipment to form NFs on the electrode-attached rotary collector. The distance between the tip of the needle and the collector was fixed. In the electrospinning process, a high voltage was applied to a solution droplet at the needle tip. Under the electrostatic interactions, the droplet was distorted with a shape of Taylor cone. Once the electric field reached a critical

value, the electrostatic force overcame the surface tension of the solution resulting in ejection of the charged liquid jet. On the way to the collector, the jet was subsequently stretched by electric forces to form a continuous and thin fiber [6, 10]. The electrospun NFs were finally annealed at 600˚C in the air for 3h.

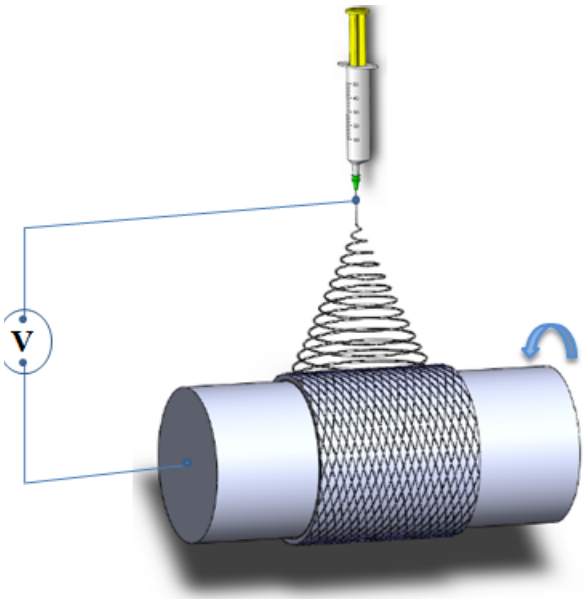

Fig. 1. Schematic illustration of synthesis of ZnO NFs using electrospinning method.

The fabricated ZnO nanofiber sensors were characterized by thermal analysis (NETZSCH STA 409 PC), FESEM (Hitachi S–4800), and XRD (D5005, Bruker – Germany). Elemental analysis was done by the EDX detector integrated in the FESEM instrument. The NO_2 gas sensing properties of the sensors were tested using a home-made gas-sensing system [11]. Resistance change under various NO_2 concentrations and operating temperatures was measured by a source meter (Keithley model 2602). Gas response is defined as $S = R_{air}/R_{gas}$, where R_{air} and R_{gas} are the resistances of the sensor in the dry air and NO_2 gas, respectively.

III. RESULTS AND DISCUSSION

The thermal stability curve for the precursor NFs of PVA/zinc acetate composites is shown in Fig. 2. There are three significant weight reduction steps occurring in the thermogravimetric (TG) curve. The first step (∼12 wt.%) between 40˚C and 140˚C is caused by the loss of residual solvent and absorbed water in the NFs. The second weight loss (∼46 wt.%) in the range of 200 – 300˚C is attributed to the decomposition of the acetate group and dehydration on the polymer side chain. It is reported that standard crystallization process normally starts at around 250˚C [12]. The third weight loss (∼20 wt.%) is due to to the continuous decomposition of zinc acetate and the main chain of PVA. For temperatures above 500˚C, there is no further change in weight loss indicating that the decomposition of the electrospun NFs is nearly complete. Therefore, we performed the thermal annealing of the NFs at 600˚C.

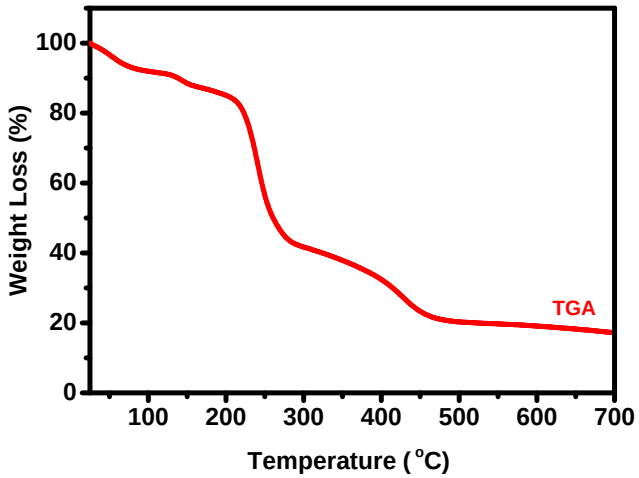

Fig. 2. TG-DTG curves of precursor fibers of PVA/Zinc acetate composite.

Fig. 3 shows the high magnification FESEM images of the as-spun and annealed nanofibers. The insets are low magnification images of both ZnO nanofiber types, which are arranged on chip like a spider's web shape. As it is exhibited in Fig. 3(a), as-spun fibers show a general feature of smooth surface. An average diameter of the as-spun fibers is about 200– 300 nm. After the thermal annealing process at 600˚C in the air, the diameter of the NFs is shrunk to 60– 100 nm as illustrated in Fig. 3(b). It can be due to the decomposition of the PVA component. Although the diameter of NFs is smaller during the calcination process, but the textures of calcined NFs was not changed. Fig. 3(b) also presents that all the individual NFs were composed of nanograins in the average size of about 20 nm.

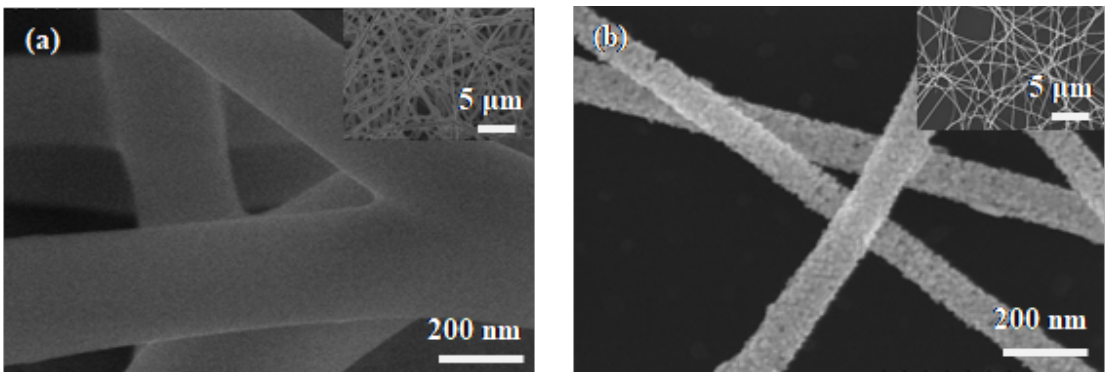

Fig. 3. SEM images of ZnO NFs (a) before calcination, (b) calcination at 600˚C.

The chemical composition of the annealed NFs was determined by the EDX spectroscopy as displayed in Fig. 4(a). The EDX spectrum indicates the presence of Zn, O elements from the NFs and Si from the substrate. It suggests that there is no impurity element integrated in the

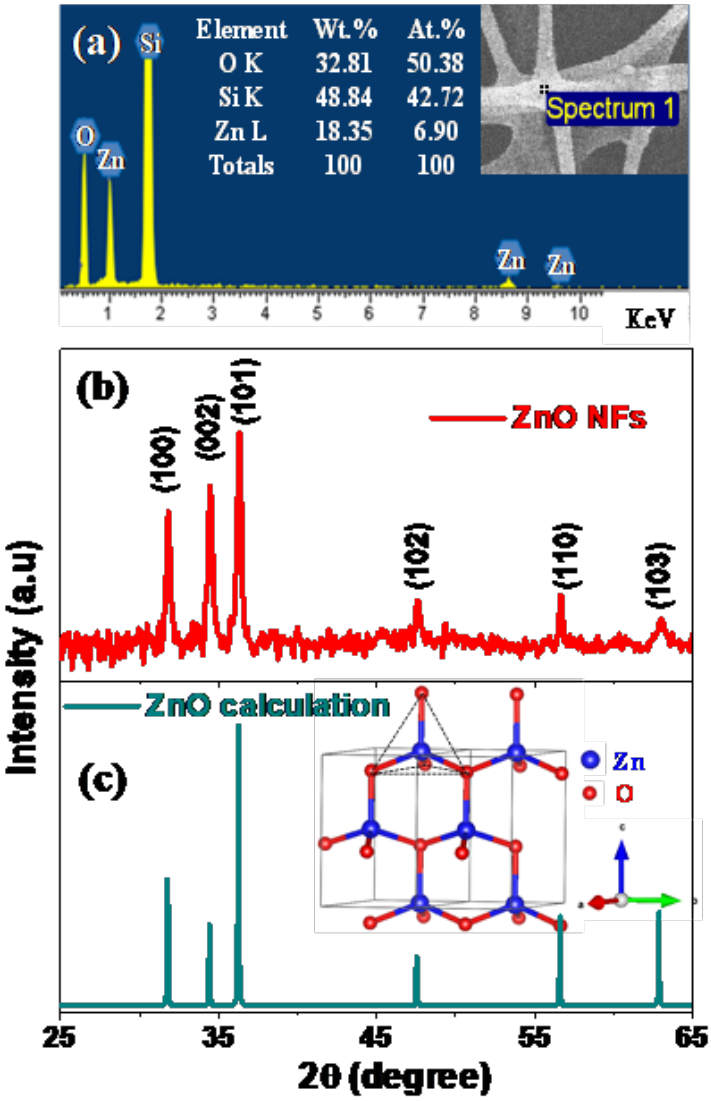

Fig. 4. (a) EDX spectroscopy of the annealed ZnO NFs. (b) and (c) are experimental and simulated XRD patterns of the annealed NFs, respectively.

synthesized NFs. To confirm the crystal structure of the annealed NFs, Fig. 4(b) and 4(c) shows the experimental and calculated XRD patterns of the annealed ZnO NFs, respectively. The XRD data calculation was carried out using the model of wurtzite ZnO (a= 3.2498 Å and c= 5.2066 Å) [13] through an open PowderCell software. A unit cell visualization of the model is shown in the inset of Fig. 4(c). It is obvious that all the experimental XRD peaks of the annealed NFs are agreed well with those of the simulated one without any additional secondary phases. This result confirms that the crystallization of the annealed ZnO NFs is in the hexagonal wurtzite structure. The average crystalline size of the ZnO NFs is calculated from the experimental XRD data using

the Scherrer equations [12]:

$$D = \frac{0.9\lambda}{\beta \cos\theta}$$

where D is the average crystalline size, λ is the X-ray wavelength (0.154 nm), θ and β are the Bragg angle and FWHM of the diffraction peak, respectively. Here, the highest peaks corresponding to reflection planes (100), (002) and (101) were used to estimate and show the average result of approximately 23.5 nm. The result is in a good agreement with the above-mentioned FESEM result.

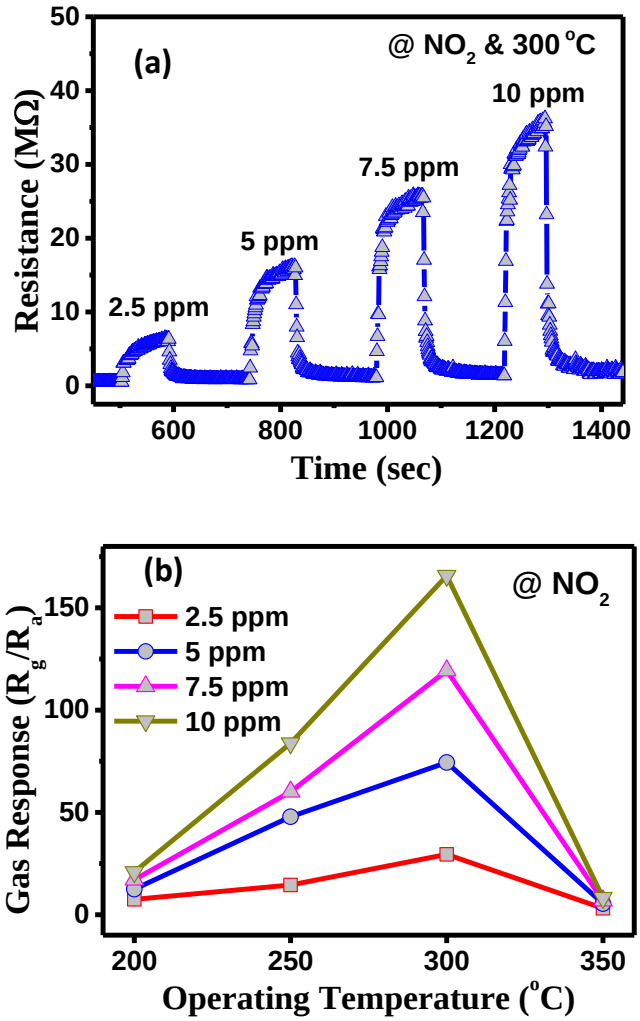

Fig. 5. (a) Dynamic resistance curves of the sensor at 300˚C and (b) sensor response of ZnO NFs as a function of the temperature (200-350 ^{o}C) and H_2 concentration (2.5-10 ppm).

In order to understand the sensing properties of the ZnO NF-based sensor, Fig. 5(a) displays the dynamic response curve of the sensor at 300˚C towards different NO_2 concentration ranges from 2.5 to 10 ppm. One can see that the resistance of the NF sensing layer is increased when the sensor is exposed to the NO_2 oxidizing gas. It reflects the n-type semiconductor nature of the synthesized ZnO NFs. Based on the R_{air} and R_{gas}, the sensor response is calculated. The gas response is 30 and 166 times on exposure of 2.5 and 10 ppm NO_2 gas, respectively. For more details, Fig. 5(b) exhibits the gas response of the ZnO NF sensor as a function of operating temperature for distinct NO_2 gas concentrations. The curves show that the response of the sensors increases with an increase in the gas concentration at all working temperature. It is evident that when the NO_2 concentration increases, the amount of NO_2 molecules absorbing on the ZnO NFs became greater leading to the increase in resistance, which enhances the sensor response. On the other hand, with all NO_2 concentrations, the sensor response goes up with an increase in working temperatures from 200 to 300˚C; then it is then decreased. The highest response of ZnO NF-based sensors is obtained at an operating temperature of 300˚C which is considered as an optimal working temperature for each NO_2 concentration.

Table 1. Comparison of the NO_2 gas sensitivity of ZnO NFs with other nanostructures.

ZnO struct. type	Conc. (ppm)	Resp. (R_g/R_a)	Temp. (˚C)	Ref.
Nanopart.	100	18	300	Ref. [14]
Nanorods	10	130	350	Ref. [3]
Tetrapod	20	20	300	Ref. [15]
NFs	10	166	300	This work

The response to NO_2 gas of ZnO NFs synthesized in this research is compared to other nanostructures of ZnO materials such as nanoparticles, nanorods, nanowires in Table 1. Obviously, NFs based sensor showed the highest response among all types of structures. This response enhancement is attributed to the formation of a large number of homojunctions at grain boundaries in the NFs.

Gas sensing mechanism of the ZnO NF-based sensors mainly depends on the change of resistivity explained by the surface depletion and grain boundary models [5, 16]. For the first model, it is well known that resistance of the ZnO NF-based sensors changes upon adsorption and desorption of target gas molecules on the sensing layer surface. Namely, when ZnO nanofibers are exposed to the air, oxygen molecules will capture electrons from the surface or the conduction band of these NFs to form oxygen ions (O_2^-, O^-, and O^{2-}), which depends on the temperature [14, 17]. For the working temperature range (200 – 350˚C) of the NF-based sensor, the oxygen ions are dominated by O_2^- or O^- [14, 17]. As the result, an electron-depleted layer is formed, and the resistance of the sensors increases. The depleted layer will be further expanded when the sensor is exposed to the NO_2 gas. Namely, the NO_2 gas is directly adsorbed on the surface, leading to formation of NO_2^- (ads) via the following reactions [1, 14, 17]:

$$NO_2(g) + e^- = NO^-_{2(ads)} \tag{1}$$

$$NO_{2(g)} + 2O^-_{(ads)} = NO^-_{2(ads)} + O_{2(g)} + e^- \tag{2}$$

$$2NO_2(g) + O^-_{2(ads)} + 2e^- = 2NO^-_{2(ads)} + 2O^-_{(ads)} \quad (3)$$

The reactions (1) and (3) dominate the reaction (2). Thus, the NO_2 gas extracts electrons from the conduction band of the surface of these NFs resulting in expansion of the depletion region and increase of the sensor resistance. With high NO_2 concentrations, the distance between $O^-_{(ads)}$ and $NO^-_{2(ads)}$ ions gets shorter. Thus, they interact each other as described in the following reaction to extract more electrons [17].

$$NO^-_{2(ads)} + 2O^-_{(ads)} + e^- = NO_{(g)} + \frac{1}{2}O_{2(g)} + 2O^{2-}_{(ads)} \quad (4)$$

Based on this mechanism, the gas sensing results of the ZnO NF sensors can be explained. The response of the sensors based on the ZnO NFs reaches to a maximum value at optimal working temperature of 300˚C for all NO_2 concentrations. When the operating temperature of the sensor increase from 200 to 300˚C, reaction rate in Eqs. (1), (2), (3) and (4) and diffusion rate of NO_2 gas along grain boundaries increase, leading to the increase in the sensor response. When the working temperature further goes up, the NO_2 desorption process will take place, resulting in a decrease in the sensor response.

Regarding the grain boundary model, we should consider the electron exchange between the nanograins on the surface layer of the NFs excluding the depletion layer. The surface layer width is the order of the Debye length [18]:

$$\lambda_D = \left(\frac{\varepsilon kT}{q^2 n_c}\right)^{\frac{1}{2}}$$

where T is absolute temperature (573K), k is the Boltzmann constant, ε is the static dielectric constant of ZnO ($= 77.438 \times 10^{-12}$ F/m), q is the electrical charge of the carrier ($1.6 \times 10^{-19}C$), and n_c is the carrier concentration (5.1×10^{16} cm^{-3}) obtained by the Hall measurement of the ZnO thin film [18]. Thus, the calculating λ_D for the NF surface layer at 300 ˚C is about 21.7 nm. It was already mentioned above that the size of the nanograins were about 20 nm. It means that the absorbed oxygen and NO_2 gases not only extract electron from a single grain, but also deplete the electron from the adjacent grains. Namely, when the sensor is exposed to the air, oxygen molecules diffuse into the NFs through the nanograins. The adsorbed oxygen-containing species tend to extract electrons from the conduction band of the nanograins resulting in the band bending and establishing the potential barriers at grain boundaries. As soon as the sensor is exposed to the NO_2 gas, which are adsorbed along grain boundaries to extract electrons from the conduction band of the nanograins, this result in further increasing height of the potential barriers leading to the raise of the NF resistance. Therefore, the response of the NF-based sensors to NO_2 gas is improved significantly in comparison with the one of the sensor based on other sensing layer structures. Fig. 6(a) reveals the response time of ZnO NF-based sensors to 2.5 ppm NO_2 as a function of the operating temperature. One can see that when the temperature raised from 200 to 350 ^{o}C, the response and recovery time rapidly decreased from 150s to 53s and from 72s to 20s, respectively. The faster response time of the sensor is due to the enhancement of reaction rate in Eq. (1–3) at higher temperatures. Meanwhile, the reaction rates of NO_2 desorption and oxygen dissociation processes are also increased at high temperature resulting in a reduction in the recovery time Similarly, Fig. 6(b) shows the response and recovery time of the sensors as a function of NO_2 gas concentration at the working temperature of 300˚C. Both the response and

recovery time are decreased by half with the increase in the gas concentration from 2.5 ppm to 10 ppm. When NO_2 concentration is increased, the time for a total adsorption of NO_2 gas on the active sites of ZnO NFs decreased, resulting in a reduction in the response time. At the same time, the products in Eq. (4) quickly desorb from ZnO NFs leading to the decrease of the recovery time.

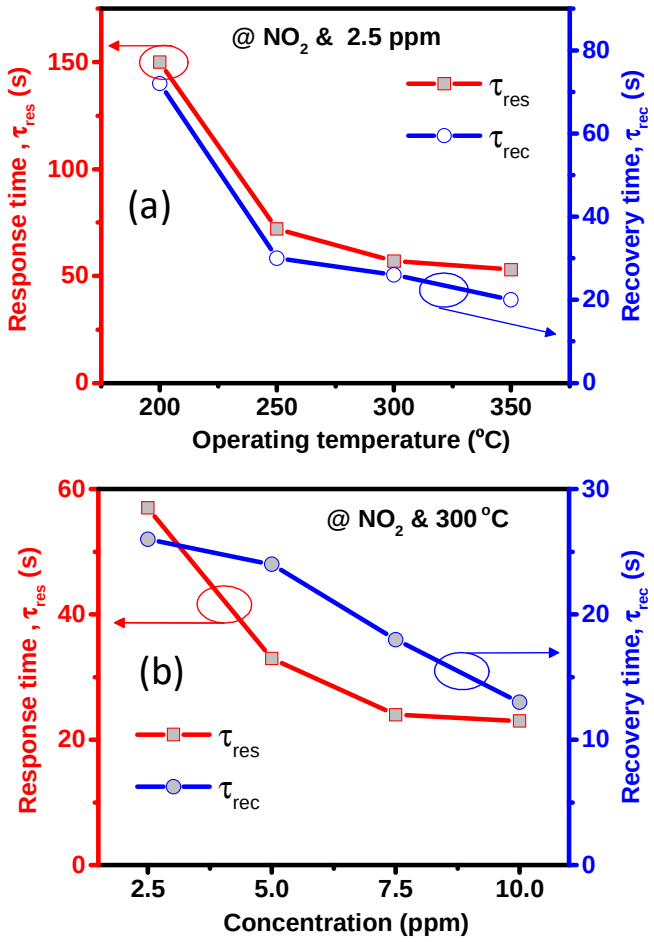

Fig. 6. Response time and recovery time of ZnO NF-based sensors as a function of operating temperature (a) and NO_2 gas concentration (b).

IV. CONCLUSION

ZnO NFs with an average diameter of 80 nm and grain size of about 23.5 nm, were successfully synthesized by the electrospinning method, followed by the annealing process. The NO_2sensors based on these NFs towards 10 ppm showed significantly high sensitivity of 166 at the optimal working temperature of 300˚C. The response and recovery time of the 10 ppm NO_2 sensor at 300˚C were as fast as of 26s and 13s, respectively. The formation of homojunctions at

the boundaries between the adjacent nanograins having the size equal to Debye length played a crucial role for the NO_2 gas response enhancement of the ZnO NF-based sensors.

ACKNOWLEDGEMENTS

This research is funded by the Vietnam National Foundation for Science and Technology Development (NAFOSTED) under Grant No. 103.02-2015.88.

REFERENCES

[1] R. Kumar, O. Al-Dossary, G. Kumar, and A. Umar, *Nano-Micro Lett.* **7** (2015) 97.
[2] I. Sayago, M. Aleixandre, and J. P. Santos, *2017 Spanish Conference on Electron Devices (CDE)*, 8-10 Feb. 2017, Barcelona, Spain.
[3] L. Shi, A. J. T. Naik, J. B. M. Goodall, C. Tighe, R. Gruar, R. Binions, I. Parkin, and J. Darr, *Langmuir* **29** (2013) 10603.
[4] M.-W. Ahn, K.-S. Park, J.-H. Heo, D.-W. Kim, K. J. Choi, and J.-G. Park, *Sensors Actuators B Chem.* **138** (2009) 168.
[5] Z. U. Abideen, A. Katoch, J. H. Kim, Y. J. Kwon, H. W. Kim, and S. S. Kim, *Sensors Actuators, B Chem.* **221** (2015) 1499.
[6] Y. Zhang, X. He, J. Li, Z. Miao, and F. Huang, *Sensors Actuators, B Chem.* **132** (2008) 67.
[7] X. Yang, C. Shao, H. Guan, X. Li, and J. Gong, *Inorg. Chem. Commun.* **7** (2004) 176.
[8] A. Katoch, S. W. Choi, H. W. Kim, and S. S. Kim, *J. Hazard. Mater.* **286** (2015) 229.
[9] T. Senthil and S. Anandhan, *J. Colloid Interface Sci.* **432** (2014) 285.
[10] A. Di Mauro, M. Zimbone, M. E. Fragal??, and G. Impellizzeri, *Mater. Sci. Semicond. Process.* **42** (2016) 98.
[11] P. Van Tong, N. D. Hoa, N. Van Duy, and N. Van Hieu, *RSC Adv.* **5** (2015) 25204.
[12] K. Thangavel, A. Balamurugan, T. Venkatachalam, and E. Ranjith Kumar, *Superlattices Microstruct.* **90** (2016) 45.
[13] A. Zeuner, H. Alves, D. M. Hofmann, B. K. Meyer, M. Heuken, J. Bläsing, A. Krost, *Appl. Phys. Lett.* **80** (2002) 2078.
[14] P. Rai and Y. T. Yu, *Sensors Actuators, B Chem.* **173** (2012) 58.
[15] D. Calestani, M. Zha, R. Mosca, A. Zappettini, M. C. Carotta, V. Di Natale, and L. Zanotti, *Sensors Actuators, B Chem.* **144** (2010) 472.
[16] H. U. Lee, K. Ahn, S. J. Lee, J. P. Kim, H. G. Kim, S. Y. Jeong, and C. R. Cho, *Appl. Phys. Lett.* **98** (2011) 11.
[17] A. Mirzaei, B. Hashemi, and K. Janghorban, J. *Mater. Sci. Mater. Electron.* **27** (2016) 3109.
[18] C. Jin, S. Park, H. Kim, and C. Lee, *Sensors Actuators B. Chem.* **161** (2012) 223.